ACS Catalysis

Research Article

pubs.acs.org/acscatalysis

Controllable Synthesis and Acetylene Hydrogenation Performance of Supported Pd Nanowire and Cuboctahedron Catalysts

Yu-Fei He, Jun-Ting Feng,* Yi-Yun Du, and Dian-Qing Li*

State Key Laboratory of Chemical Resource Engineering, Beijing University of Chemical Technology, Beijing 100029, China

Supporting Information

ABSTRACT: Supported Pd nanowire and cuboctahedron catalysts have been synthesized in an ethylene glycol−poly(vinylpyrrolidone)−KBr system using a precipitation−reduction method. KBr plays a critical role in controlling the morphology of Pd: with a variety of relatively low KBr concentrations, Pd nanowires with different lengths were obtained, but after adding sufficient KBr, shape evolution from nanowires to cuboctahedrons was observed. HRTEM images showed that the twisted Pd nanowires were actually composed of primary cuboctahedrons. Furthermore, lattice distortion was observed at interfacial regions, and the number of crystal boundaries increased with increasing length of the nanowires. The catalytic performance of the Pd materials was investigated in the selective hydrogenation of acetylene. The activities of the Pd nanowire catalysts were significantly higher than those of the cuboctahedron catalyst and gradually increased with the increasing number of crystal boundaries, indicating that the defect sites at crystal boundaries are more active owing to the exposure of larger numbers of Pd atoms. However, higher activity resulted in excessive hydrogenation and a decrease in ethylene selectivity. Therefore, the Pd cuboctahedron catalyst possessed higher selectivity. The relationship between crystal boundaries and catalytic performance was quantified, and the catalytic activity was found to increase linearly with an increasing number of crystal boundaries, whereas the trend in the selectivity was the reverse.

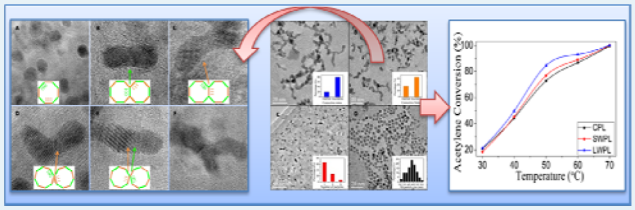

KEYWORDS: *supported Pd catalyst, nanowire, cuboctahedron, crystal boundary, defect sites, acetylene-selective hydrogenation*

1. INTRODUCTION

Ethylene is an important polymerization feedstock and intermediate in many industrial reactions. It is usually produced through thermal or catalytic cracking of higher hydrocarbons. During the process, a minute amount of acetylene is inevitably produced. The traces of acetylene in the stream can poison ethylene polymerization catalysts. Therefore, the acetylene content in the feedstock has to be reduced to a minimum of 5 ppm.[1−4] There are two general approaches (reaction and separation) to reduce the acetylene concentration in the feedstock. Selective hydrogenation is the more attractive method because of its relative ease and low cast.[5,6]

Supported noble metal catalysts are used commercially in the selective hydrogenation.[7,8] Several factors can influence the performance of supported metal catalysts, including the morphology and size of the supported metal particles, the nature of the support, and the metal−support interaction.[9−12] Recently, ways of controlling the morphology of supported metal particles have been widely studied because the morphology can significantly affect the intrinsic properties of nanoparticles and thereby influence the performance of the catalyst.

A wide variety of nanocrystals with different shapes, including cubes, wires, octahedrons, plates, icosahedrons, and pentagonal rods have been prepared by carefully controlling the reaction conditions, such as the nature of the reductants and capping agents, temperature, pH value, and concentrations of reagents and ionic species. Yang et al.[13] prepared cuboctahedral Pt nanoparticles in a $NaBH_4$−tetradecyltrimethylammonium bromide system at a low pH. By changing the pH value, the reduction rate can be well controlled, and therefore, shape evolution from cuboctahedral to cubic was observed. Xia et al.[14,15] synthesized uniform cuboctahedral nanoparticles of Pd in an ethylene glycol−poly(vinylpyrrolidone) (EG−PVP) system. When Fe^{3+} was introduced, triangular nanoplates were obtained. By altering the amount of Fe^{3+}, hexagonal nanoplates could be synthesized. In addition, they further prepared nanoscale octahedrons and nanocubes/nanobars of Ag by adding citrate and PVP as the capping agent, respectively, showing that the capping agent can also play a critical role in controlling the morphology of nanoparticles.[16]

Investigating the relationship between the morphology, especially the exposed facets, of metal nanoparticles and their catalytic performance has attracted extensive interest.[17−20] Davis and co-workers[21] found that hexagonal (111) Pt surfaces were 3−7 times more active than cubic (100) surfaces for aromatization reactions. In our previous study, tetrahedral and truncated octahedral Pd nanoparticles were controllably synthesized, and the tetrahedral particles—with only Pd (111) facets exposed—were found to exhibit a higher

Received: April 5, 2012
Revised: June 26, 2012
Published: July 3, 2012

selectivity toward the selective hydrogenation of acetylene than truncated octahedral Pd particles enclosed by Pd (111) and (100) facets.[22] Therefore, the Pd (111) facet can be regarded as the preferred facet, demonstrating that the catalytic performance of supported Pd catalysts in the selective hydrogenation of acetylene is dependent on which facet of the metal particles is exposed to the reactants.

In addition to the effect of different facets, the role of defects has also gradually attracted the interest of researchers.[23,24] Blackmond et al.[25] showed that the defect sites at edges and corners on the surface of metal nanoparticles were the active sites for the Heck reaction; however, the relationship between the defect sites of supported metal catalysts and their performance in the selective hydrogenation of acetylene has not been studied.

Layered double hydroxides (LDHs), also known as hydrotalcite-like materials, are a group of anionic clays with a layered structure. Because of their low cost, versatility, and potential ability to be recycled, LDHs have been variously used as a catalyst precursor, support, and promoter.[26−28] Nikolopoulos et al.[29] prepared Pd and Pt catalysts supported on calcined LDHs for use in acetone condensation and selective hydrogenation. Choudary et al.[30] synthesized a Pd/MgAl−LDH catalyst that exhibited high activity and selectivity for the Heck reaction. In our previous work, Pd/MgAl−LDH was prepared in situ on the surface of spherical Al_2O_3 to obtain a Pd/LDH/Al_2O_3 catalyst for the selective hydrogenation of acetylene. The presence of the LDH on the surface of the alumina enhanced the surface area, lowered the acidity, and strengthened the interaction between Pd and the alumina support.[31] It has been shown that the use of LDH as a catalyst support generates surface basic sites, which suppresses the formation of green oil and therefore improves the catalytic performance in selective hydrogenation.[32,33]

In this paper, novel supported Pd nanowire and cuboctahedron catalysts were synthesized in an EG−PVP−KBr system using the precipitation−reduction method reported in our previous work;[22] that is, the reduction of a Pd^{2+} precursor to Pd^0 accompanied by the formation of the LDH support. HRTEM was used to confirm the morphology of the resulting Pd nanocrystals, and the mechanism of the formation of the Pd nanowires was studied. The catalytic performance of Pd/LDH catalysts with different Pd morphologies was then investigated in the selective hydrogenation of acetylene, and the relationship between crystal boundaries and catalytic performances was quantified.

2. EXPERIMENTAL SECTION

2.1. Materials. $Mg(NO_3)_2{\cdot}6H_2O$, $Al(NO_3)_3{\cdot}9H_2O$, urea, $PdCl_2$, NaCl, EG, PVP, and KBr were A.R. grade and used without further purification. The water used in all the experiments was deionized and had an electrical conductivity $<10^{-6}$ S·cm^{-1}.

2.2. Preparation of Pd/LDH Catalysts. *2.2.1. Preparation of L-Wires−Pd/MgAl−CO_3−LDH Catalyst.* $PdCl_2$ was used as the Pd^{2+} precursor in the synthesis of Pd/MgAl−CO_3−LDH catalysts by the precipitation−reduction method. Solution A was prepared by dissolving 1.5384 g of $Mg(NO_3)_2{\cdot}6H_2O$, 1.1254 g of $Al(NO_3)_3{\cdot}9H_2O$, and 3.7840 g of urea in 90.0 mL of deionized water. Solution B was prepared by dissolving 0.0322 g of $PdCl_2$ and 0.0212 g of NaCl in 10.0 mL of deionized water. Solutions A and B together with 2.0 mL of EG and 0.2000 g of PVP were mixed together, and then 0.0147 g of KBr was added to the mixed solution before it was transferred into an autoclave. The autoclave was heated to 150 °C for 6 h. The decomposition of EG in aqueous solution (eq 1) and the reduction of the Pd^{2+} precursor (eq 2) occur as shown below:

$$2HOCH_2CH_2OH \rightarrow 2CH_3CHO + 2H_2O \quad (1)$$

$$PdCl_4^{2-} + 2CH_3CHO \rightarrow CH_3CO{-}OCCH_3 + Pd + 2H^+ + 4Cl^- \quad (2)$$

The autoclave was subsequently allowed to cool naturally to room temperature. The resulting precipitate was washed and filtered until the pH value of the filtrate reached 7 and then washed with acetone to remove the PVP. After drying overnight at 70 °C, a Pd/MgAl−CO_3−LDH catalyst with a $n_{Pd}/n_{Mg}/n_{Al}$ molar ratio of 2/66/33 was obtained. Since this catalyst contained long Pd nanowires, it is denoted L-wires−Pd/MgAl−CO_3−LDH (LWPL) in the subsequent discussion.

2.2.2. Preparation of M-Wires−Pd/MgAl−CO_3−LDH (MWPL) Catalyst, S-Wires−Pd/MgAl−CO_3−LDH (SWPL) Catalyst and Cuboc-Pd/MgAl−CO_3−LDH (CPL) Catalyst. The processes for the preparation of catalysts with medium length Pd nanowires, short Pd nanowires, and Pd cuboctahedrons were similar to that for the LWPL catalyst, except that 0.0294 g, 0.1470 and 0.2940 g of KBr were used, respectively.

2.3. Catalyst Characterization. The morphology, lattice fringes and crystal boundaries of the samples were examined using a JEOL JEM-2100 high-resolution transmission electron microscope (HRTEM). X-ray diffraction (XRD) patterns were recorded on a Shimadzu XRD-6000 diffractometer using Cu Kα radiation (λ = 0.154 187 nm) in the 2θ range 3−70° with a scan speed of 10° min^{-1}. To prevent oxidation, the prepared samples were sealed in a vacuum system before the X-ray photoelectron spectra (XPS) analysis. XPS of the catalysts was recorded with a Thermo VG ESCALAB 250 spectrometer equipped with Mg Kα radiation. The C 1s peak at 284.6 eV was used as a calibration peak. Elemental analysis for Pd was performed using a Shimadzu ICPS-75000 inductively coupled plasma emission spectrometer (ICP-ES), an Elementar Vario EL elemental analyzer, and a PANalytical Axios Advanced wavelength dispersive X-ray fluorescence (WDXRF) spectrometer.

H_2−O_2 titrations and H_2-temperature programmed desorption (H_2-TPD) were conducted on a Tianjin XQ TP−5000 chemisorption instrument with a thermal conductivity detector (TCD). About 100 mg of a catalyst sample was loaded in a quartz reactor. Pd dispersion of the catalysts was estimated by H_2−O_2 titration. Before H_2−O_2 titration, the catalysts were heated at 120 °C for 2 h in nitrogen and activated in a stream of 10% H_2/Ar mixture at a flow rate of 40 mL min^{-1} for 1 h at the same temperature. After this preprocess, the temperature was kept at 120 °C, and the reactor was flushed with helium at a flow rate of 40 mL min^{-1} for 0.5 h to obtain a low and stable background. Then multiple pulses of oxygen were passed over the catalyst from a 50 μL loop at 120 °C until a constant O_2 peak area was observed. After changing the carrier gas to nitrogen, the flow rate was then maintained at 40 mL min^{-1} for 0.5 h. After obtaining a stable background, multiple pulses of hydrogen were passed over the catalyst from a 50 μL loop until a constant H_2 peak area was observed. After repeating this process several times, the Pd dispersion was calculated according to the following formula:[34]

dx.doi.org/10.1021/cs300224j | ACS Catal. 2012, 2, 1703−1710

$$D(\%) = \frac{2 \times V_T^H \times M \times 10^{-3}}{3 \times 22.4 \times W \times P} \times 100$$

where D(%) = the dispersion of Pd, V_T^H = the volume of H_2 used for the titration of O_2 (mL), M = the relative molecular mass of Pd, W = mass of catalyst (g), and P = Pd mass fraction of the catalyst (%).

Prior to H_2-TPD, the catalysts were also heated at 120 °C for 2 h in nitrogen and then placed in 10% H_2/Ar with a flow rate of 40 mL min^{-1} for 0.5 h at 30 °C. TPD was carried out in a stream of argon with a flow rate of 40 mL min^{-1} and a temperature ramp of 10 °C min^{-1}.

Vapor phase hydrogenation of acetylene was carried out in a Xian Quan WFS-3015 fixed bed microreactor over the temperature range 20−80 °C, with a space velocity (GHSV) of 8040 h^{-1}, total flow rate of 167.6 mL min^{-1}, and reaction pressure of 0.4 MPa. A 0.04 portion of catalyst and 1.96 g (1.25 mL) of quartz sand were mixed and loaded at the center of the reactor. Before reaction, the samples were activated by hydrogen at a flow rate of 5 mL min^{-1} at 100 °C for 1 h. The reactant stream contained 0.947% acetylene in ethylene, and the H_2/acetylene ratio was 1.9. The reactants and products were analyzed by gas chromatography (GC) with a flame ionization detector online using a PLOT capillary column (0.53 m × 50 mm). Acetylene conversion, ethylene selectivity, and ethane formation are defined as follows:[35]

$$\text{acetylene conversion} = \frac{C_2H_2(\text{inlet}) - C_2H_2(\text{outlet})}{C_2H_2(\text{inlet})}$$

$$\text{selectivity toward ethylene} = \frac{C_2H_4(\text{outlet}) - C_2H_4(\text{inlet})}{C_2H_2(\text{inlet}) - C_2H_2(\text{outlet})}$$

$$\text{ethane formation (mol \%)} = \frac{C_2H_6(\text{outlet})}{C_2H_2(\text{outlet}) + C_2H_4(\text{outlet}) + C_2H_6(\text{outlet})}$$

3. RESULTS AND DISCUSSION

3.1. Morphology of Supported Pd Nanoparticles. Like other face-centered cubic (fcc) noble metals, the thermodynamically favorable shapes of Pd nanocrystals are cuboctahedron and multiply twinned particles. To obtain an anisotropic nanostructure and induce new shapes, impurities or capping agents are generally employed to alter the surface free energies of nanoparticles.[36] Bromide ions have been widely employed as a capping agent. When bromide ions are introduced into the reaction system, they are able to chemisorb onto the surface of Pd seeds and alter the relative order of surface free energies.[37] Therefore, bromide ions were introduced in this work to obtain new shapes of Pd nanoparticles. In addition, PVP was employed as a stabilizing agent to prevent the aggregation of particles. When a trace of bromide ions was present, Pd nanowires with a length of over 30 nm, dispersed homogenously on the surface of the LDH support, were obtained (Figure 1A). By altering the amount of bromide ions, the length of the nanowires can be effectively controlled. As shown in Figure 1B and C, catalysts with shorter Pd nanowires were obtained by introducing more bromide ions. At even higher bromide concentrations, well-dispersed cuboctahedral Pd nanoparticles with an average size of 4.5 nm can be observed on the LDH surface, as shown in Figure 1D. Bromide ions therefore clearly play a critical role in the formation of Pd nanostructures. PVP also plays an important role in the preparation of the catalysts. The active species in all the catalysts are evenly distributed on the LDH surface, as shown in the HRTEM images in Figure 1.

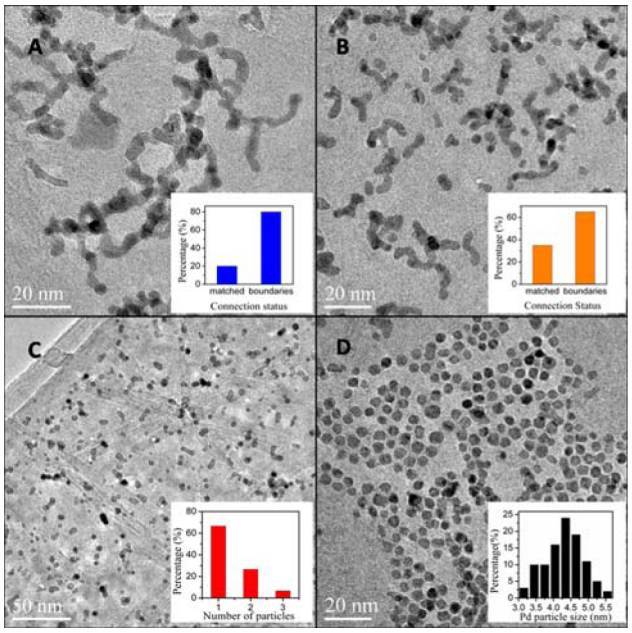

Figure 1. HRTEM images of LWPL (A), MWPL (B), SWPL (C), and CPL (D) supported on LDH surfaces. Insets in A and B are histograms of the connection status of two primary particles. Inset in C is a histogram of the number of primary particles in an extended nanocrystal. Inset in D is a histogram of Pd particle size.

The histograms in the Figure 1 insets reveal the changes in the quantity of crystal boundaries. As the length of the nanowires decreases, the ratio of crystal boundaries to joint interfaces decreases. In particular, the cuboctahedral Pd nanoparticles are monodisperse, and no crystal boundaries are observed. In this system, the chemisorbed bromide layer prevents further addition of Pd atoms from solution onto the nanocrystal surface.[38] Subsequently, oxidative etching, which is caused by oxygen (from the air) and chloride (from $PdCl_4^{2-}$), removed some of the bromide from the surface to form anisotropic nanoparticles.[14,15] However, the degree of oxidative etching is limited by the amount of residual air and $PdCl_4^{2-}$ precursor in the autoclave. Therefore, the length of the Pd nanowires is highly dependent on the amount of bromide ions.

On the basis of the HRTEM images, the Pd nanowires are composed of several single-crystalline elongated primary nanostructures, and the primary particles adopted the cuboctahedron geometry with well-defined planar facets. To better illustrate the formation of nanowires, four models with different connected facets were compared, as shown in Figure 2: (100) connected with (100), (111) connected with (111), (111) connected with (111) at an angle, and (100) connected with (111). When a (100) plane connected with another (100) plane or a (111) plane with another (111) plane, a single crystal nanowire was formed, as shown in Figure 2B and C. In contrast, when (111) planes were attached at an angle or a (100) plane attached to a (111) plane, this generated a polycrystalline nanowire, as shown in Figure 2D and E. In the case of the last two models, lattice distortion can be clearly seen in the interfacial regions where crystal boundaries existed. The four models consider only the linking of two particles, and the

dx.doi.org/10.1021/cs300224j | ACS Catal. 2012, 2, 1703−1710

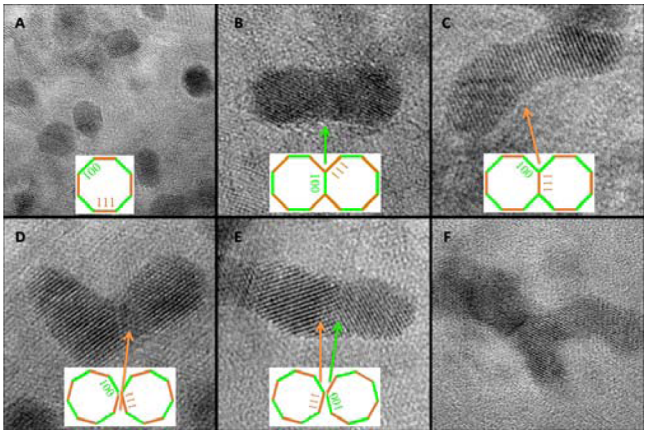

Figure 2. HRTEM images and models of primary particles (A), short nanowires of (100) connected with (100) (B), (111) connected with (111) (C), (111) connected with (111) at an angle (D), (111) connected with (100) (E), and long nanowires (F).

result of more particles' becoming attached together to form nanowires is shown in Figure 2F. As the amount of linked particles increases, the nanowires elongate and become more tortuous. Therefore, the ratio of crystal boundaries increases.

3.2. XRD, XPS, and H_2-TPD of the Supported Pd Catalysts. Figure 3 shows the XRD patterns of MgAl−CO_3−

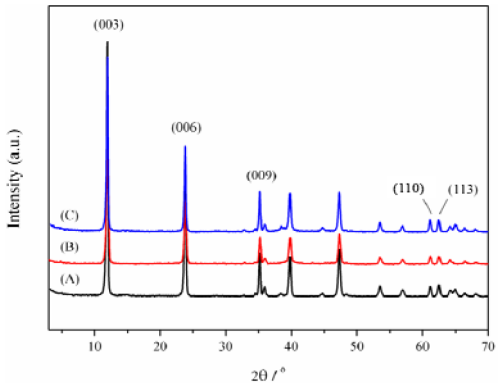

Figure 3. XRD patterns of MgAl−CO_3−LDH (A), LWPL catalyst (B), and CPL catalyst (C).

LDH (A), LWPL catalyst (B), and CPL catalyst (C). The pattern in part A is similar to that previously reported for an LDH with intercalated CO_3^{2-} anions (JCPDS 89-0460); the MgAl−CO_3−LDH sample displays the characteristic reflections of the LDH structure with a series of (00 L) peaks at low angle and nonbasal reflections (h, $k \neq 0$) at high angle, showing a high crystallinity. The d_{003} basal spacing of the LDH support is 7.6 Å, which is in accordance with the literature value.[39] In Figure 3, traces B and C, the LDH diffraction peaks and the d_{003} basal spacing are essentially identical to those in trace A. This suggests that the addition of $PdCl_4^{2-}$ anions has little influence on the crystalline nature of MgAl−CO_3−LDH and that the Pd particles are mainly located at the surface or the edge-on surfaces of MgAl−CO_3−LDH rather than in the interlayer galleries.[30] However, the reflections of Pd were not observed, which can be attributed to the small particle size and relatively low Pd loading in LWPL and CPL catalysts.

Figure 4 displays the Pd 3d XPS spectra of LWPL catalyst, SWPL catalyst, and CPL catalyst. The peaks at ~335.2 and

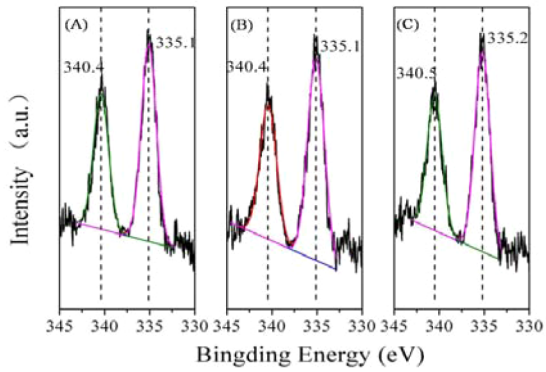

Figure 4. Pd 3d XPS spectra of LWPL catalyst (A), SWPL catalyst (B), and CPL catalyst (C).

~340.4 eV are in accordance with the literature values for Pd $3d_{5/2}$ and Pd $3d_{3/2}$ of bulk Pd^0.[40−42] Peaks characteristic of Pd(II) compounds were not observed in the spectra, indicating that all the Pd^{2+} precursor has been reduced to Pd^0. It is well-known that species such as Br^- and Cl^- anions remaining in catalysts can poison the active sites. EDX and WDXRF analysis were therefore performed to monitor the amount of residual Br^- and Cl^- capping agents. No signals of Br^- and Cl^- were detected in the EDX tests of CPL catalyst and SWPL catalyst (Supporting Information Figure S1). To confirm these results, WDXRF spectra were also recorded, and the ratios of Pd/Br or Pd/Cl in all catalysts were found to be higher than 198. The above results show that the Br^- and Cl^- capping agents have been efficiently removed from the surface of the supported Pd nanoparticles by extensive washing.

H_2-TPD experiments were carried out on the pristine MgAl−CO_3−LDH support and Pd/MgAl−CO_3−LDH catalysts to gain information about H_2 activation/dissociation; the results are shown in Figure 5. The broad peak at ~95 °C in the profile

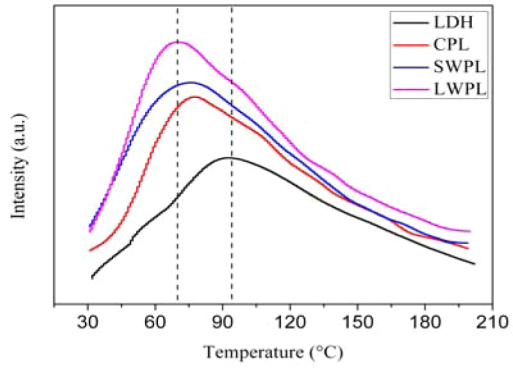

Figure 5. H_2-TPD profiles of MgAl−CO_3−LDH support, CPL catalyst, SWPL catalyst, and LWPL catalyst.

for the LDH precursor is caused by the desorption of H_2 from the LDH surface. The profiles of CPL, SWPL, and LWPL catalyst, however, show a main peak and a small broad hump. The hump can be ascribed to the desorption of H_2 from the LDH support. The main H_2 desorption peak results from chemisorbed hydrogen and the decomposition of hydride species associated with Pd.[43,44] It should be noted that the amount of hydrogen chemisorbed on the LWPL catalyst with the long nanowires was the highest, whereas the T_{max} value was the lowest for this material. This indicates that in the case of the

dx.doi.org/10.1021/cs300224j | ACS Catal. 2012, 2, 1703−1710

long Pd nanowires, H_2 dissociation/activation occurred most readily, and the amount of activated H was a maximum, which can be attributed to there being more exposed Pd atoms at the crystal boundaries, resulting from the larger number of defects. Spillover of hydrogen to the support is not taken into account because of the high desorption temperature of spillover hydrogen (≥503 K) and our relatively mild reaction conditions.[44]

3.3. Selective Hydrogenation of Acetylene. The performances of the catalyst samples in the selective hydrogenation of acetylene in an ethylene-rich stream were compared using a fixed-bed flow reactor. The Pd loading and dispersion in the catalysts, obtained from H_2−O_2 titration analysis, are listed in Table 1. The experimental Pd loadings employed in the final catalysts are slightly different from those in the corresponding synthesis mixture (2.5 wt.%), but the values are reproducible within experimental error. The Pd dispersion decreased in the order LWPL catalyst > SWPL catalyst > CPL catalyst. In addition, the number of crystal boundaries decreases in the order LWPL catalyst > SWPL catalyst > CPL catalyst, as shown in Figure 1. These results confirm that the larger number of crystal boundaries and increased number of defects give rise to more exposed Pd atoms, as reported previously.[18,43,45] Figure 6 shows plots of the acetylene conversion and ethylene selectivity versus reaction temperature for LWPL catalyst, SWPL catalyst, and CPL catalyst. The acetylene conversion increases with increasing reaction temperature, and the ethylene selectivity decreases. The two catalysts containing Pd nanowires exhibit higher acetylene conversion than that of the CPL catalyst containing cuboctahedral Pd nanoparticles.

Table 1. Properties of the Catalysts (T = 25°C, GHSV = 8040 h^{-1})

catalyst	CPL	SWPL	LWPL
Pd loading (%)[a]	2.37	2.36	2.35
Pd dispersion (%)[b]	27.9	29.2	33.1
BE of Pd 3d (eV)			
$3d_{5/2}$, $3d_{3/2}$	335.2, 340.5	335.1, 340.4	335.1, 340.4
T_{max} of H_2 desorption[c] (°C)	77	75	70
Acetylene conversion (%)	13.79	8.25	8.91
TOF (s^{-1})	0.0217	0.0125	0.0118

[a]Determined by ICP analysis. [b]Determined by H_2−O_2 titration analysis. [c]Determined by H_2-TPD.

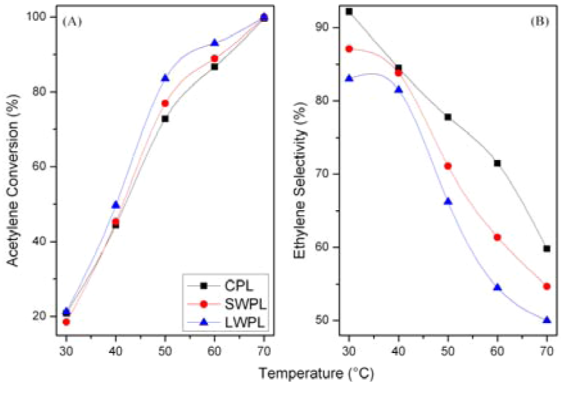

Figure 6. Plots of acetylene conversion (A) and ethylene selectivity (B) versus reaction temperature over different catalysts with total pressure of 0.4 MPa, GHSV of 8040 h^{-1}, 33.2% C_2H_4/C_2H_2 mixed gases (containing 0.947% acetylene in ethylene), 0.6% H_2, and 66.2% N_2 (H_2/C_2H_2 = 1.9).

In this work, catalytic activity is defined as the rate of acetylene consumption, which is expressed as the number moles of acetylene converted in unit time. Therefore, higher acetylene conversion represents higher rate/activity. The reason why the catalysts with Pd nanowires possess higher activity can be attributed to their special structure. The twisted nanowires are endowed with numerous crystal boundaries, where numerous defects are collected. Thus, more crystal boundaries lead to the exposure of a larger number of Pd atoms and, therefore, a higher Pd dispersion. This can also explain why the catalysts containing Pd nanowires have higher amounts of hydrogen chemisorption and lower T_{max} values for the desorption, as listed in Table 1. The LWPL catalyst exhibited the highest activity due to its largest capacity for hydrogen activation/dissociation.

TOF, as the intrinsic activity of the reaction, is calculated at 25 °C and is expressed as the rate of acetylene consumption per number of exposed Pd sites on the catalyst.[46] The TOF values of the catalysts (listed in Table 1) are comparable to those of other reported Pd catalysts under similar reaction conditions[22,47] but do vary somewhat with the Pd dispersion. This indicates that the acetylene hydrogenation reaction is structure-sensitive, which is in accord with the literature.[48,49] Although there may be some poisoning of the active sites by residual Br^- and Cl^- anions, since the concentrations of $Br^-$and Cl^- are at parts per million levels, any poisoning effect is unlikely to outweigh the effect of defects. Therefore, the poisoning of the active sites by residual Br^- and Cl^- anions has not been considered in this work.

The Koros−Nowak test is an effective method to identify heat or mass transfer limitations in the measurement of catalytic rates.[50,51] If the observed TOFs of catalysts with different loadings are the same, this means that there are no heat or mass transfer limitations under the tested conditions. Therefore, a Koros−Nowak test was carried out on catalysts with similar dispersion but different Pd loadings at 25 °C. As shown in Figure 7, the values of TOF remain almost unchanged under the same reaction conditions when altering the Pd loading, demonstrating that there are no heat or mass transfer limitations under this condition. On this basis, the apparent activation energy (E_a) values for the different catalysts were obtained by plotting ln TOF versus 1/T, as shown in Figure 8.

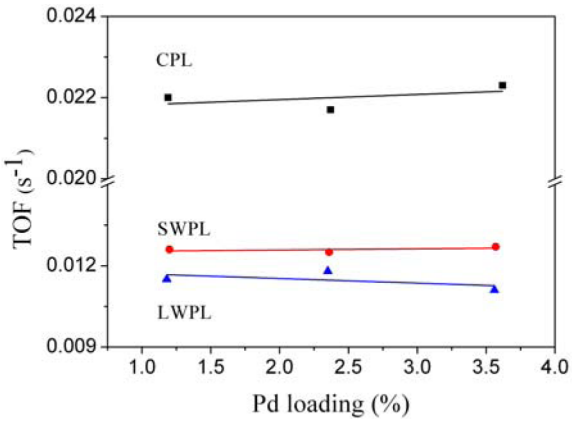

Figure 7. Plots of TOF versus Pd loading for different catalysts at 25 °C.

dx.doi.org/10.1021/cs300224j | ACS Catal. 2012, 2, 1703−1710

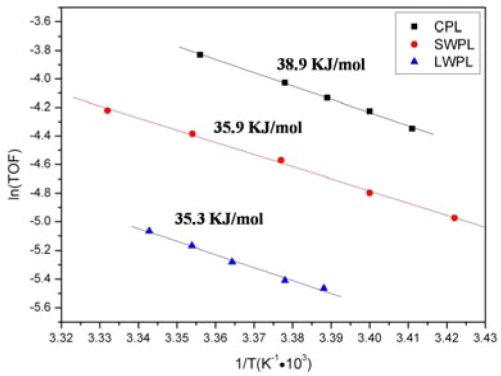

Figure 8. Plots of the natural logarithm of TOF versus inverse temperature, showing the apparent activation energy at low temperatures.

The values of E_a for the three catalysts are well within the range of reported values (30.0−65.0 kJ/mol) for this reaction,[47,52,53] and the accuracy of fitting a straight line was more than 99.9% in each case. The value of E_a increased in the order LWPL < SWPL < CPL, suggesting that the presence of crystal boundaries can lower the activation barrier of the reaction and give an increase in hydrogenation activity.[54]

In a selective hydrogenation reaction, the activity of a catalyst is not the only important parameter. In a series reaction of the type A → B → C (where A represents acetylene; B, ethylene; and C, ethane), the selectivity of formation of B is also important.[55,56] As shown in Figure 6B, the ethylene selectivity of the three catalysts decreased with increasing temperature. It is worth noting that the CPL catalyst displayed the highest selectivity toward ethylene of the three catalysts in the temperature range from 30 to 70 °C. Since ethylene is produced as an intermediate in the acetylene hydrogenation reaction, when the acetylene conversion approached 100%, the selectivity toward ethylene decreased dramatically. It is therefore necessary to compare the performance of different catalysts at similar conversions.

In Figure 9A, the selectivity toward ethylene decreased with increasing acetylene conversion for all three catalysts. For the same conversion, the CPL catalyst exhibited higher selectivity toward ethylene than the SWPL and LWPL catalysts. As for the

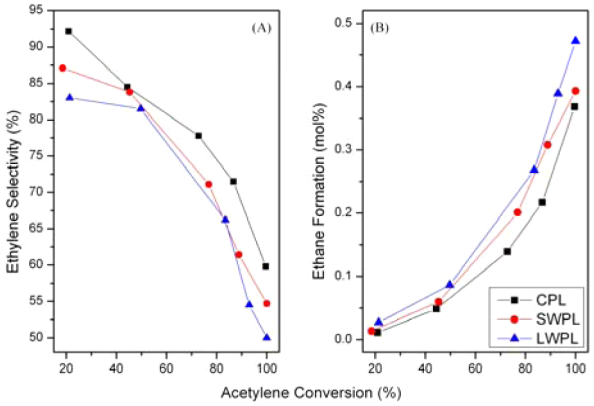

Figure 9. Plots of ethylene selectivity and ethane formation versus acetylene conversion over different catalysts with total pressure of 0.4 MPa, GHSV of 8040 h^{-1}, 33.2% C_2H_4/C_2H_2 mixed gases (containing 0.947% acetylene in ethylene), 0.6% H_2, and 66.2% N_2 (H_2/C_2H_2 = 1.9).

catalyst with Pd nanowires, more molecular H_2 was activated (as observed by H_2−TPD), which facilitates the hydrogenation of unsaturated hydrocarbon. In addition, the adsorption strength of ethylene has a major effect on the selectivity.[57,58] For a given metal, the adsorption strength varies in the same order: aromatic < olefin < diolefin < alkyne. On the basis of the known "volcano" curve, the maximum value of the activity of the metal as a function of the adsorption strength is located between that for olefins and diolefins.[59] For the selective hydrogenation of acetylene, defects at crystal boundaries with high surface energy increase the adsorption strength of both acetylene and ethylene.[60] An increase in adsorption strength of acetylene would reduce the activity of acetylene hydrogenation, but because of the exposure of a larger amount of Pd atoms, the effect of stronger adsorption of acetylene is obscured. However, an increase in the adsorption strength of ethylene improves the activity of ethylene hydrogenation, resulting in a decline in ethylene selectivity. This is consistent with the experiment plots of ethane formation versus acetylene conversion shown in Figure 9B.

Selectivity at a fixed conversion was also compared for the catalysts studied here and those in the state-of-the-art literature. At 80% acetylene conversion, the selectivities of LWPL, SWPL, and CPL catalyst were 68%, 69%, and 74.5%, respectively. It is necessary to point out that both our catalyst with Pd cuboctahedrons and that with Pd nanowires possess higher selectivity than those reported in the literature for Pd/SiO_2 (20%), $Pd-Ti/SiO_2$ (37.5%), and Pd/Zn-modified Al_2O_3 (64%) catalysts prepared by solvothermal methods at the same conversion.[61,62] However, the selectivity can be improved through modifying the activity species, and higher ethylene selectivity (≥90%) at 80% acetylene conversion was obtained by this method.[63,64]

The above results suggest that the presence of crystal boundaries, especially the defect sites in the catalysts, can significantly affect the catalytic properties. To further clarify the effect of crystal boundaries, the quantitative relation between the number of crystal boundaries and catalytic properties was investigated. The number of crystal boundaries is directly linked to the number of basic building units. As illustrated in the HRTEM images (Figures 1 and 2), Pd nanowires are composed of several single-crystalline cuboctahedral basic building units with similar size, and the number of basic building units in all the catalysts is roughly the same. A total of 200 basic building units were used to calculate the ratios of crystal boundaries: basic building units by statistical method. In addition, the number of building units in one nanowire and the connection status of the joint interface are taken into account. The computational process is summarized in Table 2. For every single basic building unit, the number of linked crystal boundaries increases from 0 (CPL catalyst) to 0.69 (LWPL catalyst).

The quantitative relationship between the ratio of crystal boundaries/basic building units and catalytic performance is shown in Figure 10. At temperatures from 30 to 50 °C, acetylene conversion of the four catalysts increased linearly with the increasing ratio of crystal boundaries/basic building units; however, the ethylene selectivity decreased. Interestingly, the selectivity toward ethylene dramatically decreased along with the appearance of crystal boundaries, indicating that the defects at crystal boundaries facilitate the overhydrogenation to ethane. In the case of the Pd nanowire catalysts, the plot of the ethylene selectivity is linear. Overall, the CPL catalyst containing

dx.doi.org/10.1021/cs300224j | ACS Catal. 2012, 2, 1703−1710

Table 2. Statistical Analysis of the Crystal Boundary/Basic Building Unit Ratio

catalyst	ratio of single particles/ total basic building units (%)[a]	no. of particles in a single nanowire[b]	ratio of crystal boundaries/ joint interfaces (%)[c]	no. of crystal boundaries	ratio of crystal boundaries/basic building units (%)
CPL	98				
SWPL	66	2.2	50	18	9
MWPL	2	5.1	67	107	53
LWPL	0	7.0	80	137	69

[a]The status of basic building units is obtained by counting ~200 units. [b]The average number of basic building units in a single nanowire is obtained by counting ~200 basic building units or 50 nanowires. [c]The connection status of joint interfaces is obtained by counting ~200 joint interfaces.

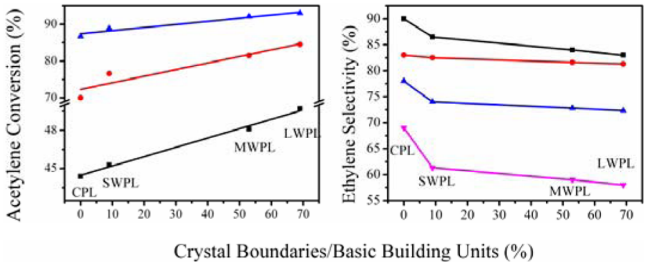

Figure 10. Quantitative relationship between crystal boundaries/basic building units and acetylene conversion (A) at 40 °C (■), 50 °C (●), and 60 °C (▲). Relation between crystal boundaries/basic building units and ethylene selectivity (B) at 30% (■), 50% (●), 70% (▲), and 90% (▼) conversion of acetylene.

uniform Pd cuboctahedrons exhibits higher ethylene selectivity, whereas the catalysts containing Pd nanowires possess higher catalytic activity, owing to the existence of defect sites at crystal boundaries. The results have great significance for the controllable synthesis of supported metal catalysts and the relationship between the morphology of the supported metal and the catalytic performances of a material in other selective hydrogenation reactions.

4. CONCLUSIONS

Novel supported catalysts containing Pd nanowires and cuboctahedrons have been synthesized in an EG−PVP−KBr system using a precipitation−reduction method. The morphology of Pd nanocrystals can be effectively controlled by introducing different amounts of KBr. When a trace of bromide was introduced, catalysts containing long Pd nanowires were obtained. On increasing the amount of KBr, the length of the nanowires decreased. Cuboctahedral Pd nanoparticles were prepared by further increasing the concentration of KBr. HRTEM images showed that the Pd nanowires were composed of several single-crystalline elongated primary cuboctahedron particles, and four possible growth models of the Pd nanowires have been presented. In the polycrystalline nanowires, a lattice distortion was clearly observed at the interfacial regions, and the number of crystal boundaries increased with increasing length of the nanowires. The morphology effect of Pd nanocrystals was investigated in the selective hydrogenation of acetylene. Compared with the CPL catalyst with cuboctahedral Pd nanoparticles, the LWPL catalyst containing Pd nanowires possessed higher Pd dispersion, higher capacity of H_2 activation/dissociation, and lower activation energy. Therefore, LWPL catalysts displayed a higher catalytic activity at the same reaction temperature. The relationship between the number of crystal boundaries and the catalytic performance was quantified, and then the effect of defects was demonstrated. With the increasing number of crystal boundaries, the hydrogenation activity of the Pd nanowires gradually increased, which indicates that the defect sites at crystal boundaries are more active owing to the exposure of larger amounts of Pd atoms. However, higher catalytic activity of the catalysts containing Pd nanowires resulted in excessive hydrogenation and a decrease in the selectivity toward ethylene. Therefore, the CPL catalyst possessed higher selectivity toward ethylene. The effects of morphology—in particular, the defect sites at crystal boundaries—on the catalytic performance have great significance for the design and synthesis of other selective hydrogenation catalysts.

■ ASSOCIATED CONTENT

Supporting Information

EDX spectra are given in Figure S1. This material is available free of charge via the Internet at http://pubs.acs.org.

■ AUTHOR INFORMATION

Corresponding Author

*Address: Box 98, 15 Bei San Huan East Road, Beijing 100029, China. Phone: +86 10 64436992. Fax: +86 10 64425385. E-mail: fengjt@mail.buct.edu.cn (J.T.F.), lidq@mail.buct.edu.cn (D.Q.L.).

Notes

The authors declare no competing financial interest.

■ ACKNOWLEDGMENTS

This work was supported by the 973 Project (2011CBA00506), the Support Plan Project (2012BAE06B08), the Doctoral Program of the Ministry of Education, and the Fundamental Research Funds for the Central Universities.

■ REFERENCES

(1) Mei, D. P.; Sheth, A.; Neurock, M.; Smith, C. M. *J. Catal.* **2006**, *242*, 1−15.
(2) Trimm, D. L.; Liu, I. O. Y.; Cant, N. W. *Appl. Catal., A* **2010**, *374*, 58−64.
(3) Zea, H.; Lestera, K.; Datye, A. K.; Rightor, E.; Gulotty, R.; Waterman, W.; Smith, M. *Appl. Catal., A* **2005**, *282*, 237−245.
(4) Feng, J. T.; Ma, X. Y.; Evans, D. G.; Li, D. Q. *Ind. Eng. Chem. Res.* **2011**, *50*, 1947−1954.
(5) Huang, W.; Pyrz, W.; Lobo, R. F.; Chen, J. G. *Appl. Catal., A* **2007**, *333*, 254−263.
(6) Vincent, M. J.; Gonzalez, R. D. *Appl. Catal., A* **2001**, *217*, 143−156.
(7) Hub, S.; Hilaire, L.; Touroude, R. *Appl. Catal.* **1988**, *36*, 307−322.
(8) Panpranot, J.; Tangjitwattakorn, O.; Praserthdam, P.; Goodwin, J. G. *Appl. Catal., A* **2005**, *292*, 322−327.
(9) Lee, I.; Delbecq, F.; Morales, R.; Albiter, M. A.; Zaera, F. *Nat. Mater.* **2009**, *8*, 132−138.
(10) Kang, J. H.; Shin, E. W.; Kim, W. J.; Park, J. D; Moon, S. H. *J. Catal.* **2002**, *208*, 310−320.
(11) Ruta, M.; Semagina, N.; Minsker., L. K. *J. Phys. Chem. C* **2008**, *112*, 13635−13641.
(12) Choo, H.; He, B.; Liew, K. Y.; Liu, H.; Li, J. *J. Mol. Catal. A: Chem.* **2006**, *244*, 217−228.
(13) Lee, H.; Habas, S. E.; Kweskin, S.; Butcher, D; Somorjai, G. A.; Yang, P. D. *Angew. Chem.* **2006**, *118*, 7988−7992.

(14) Xiong, Y.; Chen, J.; Wiley, B.; Xia, Y. *J. Am. Chem. Soc.* **2005**, *127*, 7332−7333.
(15) McLellan, J. M.; Yin, Y.; Li, Z.; Xia, Y. *J. Am. Chem. Soc.* **2005**, *127*, 17118−17127.
(16) Zeng, J.; Zheng, Y. Q.; Rycenga, M.; Tao, J.; Li, Z. Y.; Zhang, Q.; Zhu, Y. M.; Xia, Y. *J. Am. Chem. Soc.* **2010**, *132*, 8552−8553.
(17) Schmidt, E.; Vargas, A.; Mallat, T.; Baiker, A. *J. Am. Chem. Soc.* **2009**, *131*, 12358−12367.
(18) Yang, Y. W.; Unsworth, L. D.; Semagina, N. *J. Catal.* **2011**, *281*, 137−146.
(19) Berhault, G.; Bisson, L.; Thomazeau, C.; Verdon, C.; Uzio, D. *Appl. Catal., A* **2007**, *327*, 32−43.
(20) Zhang, F. X.; Chen, J. X.; Zhang, X.; Gao, W. L.; Jin, R. C.; Guan, N. J.; Li, Y. Z. *Langmuir* **2004**, *20*, 9329−9334.
(21) Davis, S. M.; Zaera, F.; Somorjai, G. A. *J. Catal.* **1984**, *85*, 206−223.
(22) Feng, J. T.; Ma, X. Y.; He, Y. F.; Evans, D. G.; Li, D. Q. *Appl. Catal., A* **2012**, *413*−*414*, 10−20.
(23) Zaera, F. *Chem. Record* **2005**, *5*, 133−144.
(24) Attard, G. A.; Griffin, K. G.; Jenkins, D. J.; Johnston, P.; Wells, P. B. *Catal. Today* **2006**, *114*, 346−352.
(25) Bars, J. L.; Specht, U.; Bradley, J. S.; Blackmond, D. G. *Langmuir* **1999**, *15*, 7621−7625.
(26) Shen, J. Y.; Guang, B.; Tu, M.; Chen, Y. *Catal. Today* **1996**, *30*, 77−82.
(27) Feng, J. T.; Lin, Y. J.; Evans, D. G.; Duan, X.; Li, D. Q. *J. Catal.* **2009**, *266*, 351−358.
(28) Tu, M.; Shen, J. Y.; Chen, Y. *J. Solid State Chem.* **1997**, *128*, 73−79.
(29) Nikolopoulos, A. A.; Jang, B. W. L.; Spivey, J. *J. Appl. Catal., A* **2005**, *296*, 128−136.
(30) Choudary, M. B.; Madhi, S.; Chowdari, N. S.; Kantam, M. L.; Sreedhar, B. *J. Am. Chem. Soc.* **2002**, *124*, 14127−14136.
(31) Ma, X. Y.; Chai, Y. Y.; Evans, D. G.; Li, D. Q.; Feng, J. T. *J. Phys. Chem. C* **2011**, *115*, 8693−8701.
(32) Wang, Q.; O'Hare, D. *Chem. Rev.* dx.doi.org/10.1021/cr200434v.
(33) Wongwaranon, N.; Mekasuwandumrong, O.; Praserthdama, P.; Panpranot, J. *Catal. Today* **2008**, *131*, 553−558.
(34) Paryjczak, T.; Jó'zwiak, K. *J. Chromatogr.* **1975**, *111*, 443−447.
(35) Vincent, M. J.; Gonzalez, R. D. *Appl. Catal., A* **2001**, *217*, 143−156.
(36) Pimpinelli, A.; Villain, J. *Physics of Crystal Growth*; Cambridge University Press: Cambridge, UK, 1998.
(37) Schimpf, J. A.; Abreu, J. B.; Soriaga, M. P. *J. Electroanal. Chem.* **1994**, *364*, 247−249.
(38) Xiong, Y.; Cai, H.; Wiley, B. J.; Wang, J.; Kim, M. J.; Xia, Y. *J. Am. Chem. Soc.* **2007**, *129*, 3665−3675.
(39) Ogawa, M.; Kaiho, H. *Langmuir* **2002**, *18*, 4240−4242.
(40) Gniewek, A.; Trzeciak, A. M.; Ziółkowski, J. J.; Kepiński, L.; Wrzyszcz, J.; Tylus, W. *J. Catal.* **2005**, *229*, 332−343.
(41) Wang, F.; Lu, G. X. *J. Phys. Chem. C* **2009**, *113*, 17070−17075.
(42) Demoulin, O.; Rupprechter, G.; Seunier, I.; Clef, B. L.; Navez, M.; Ruiz, P. *J. Phys. Chem. B* **2005**, *109*, 20454−20462.
(43) Zhang, Z. C.; Zhang, X.; Yu, Q. Y.; Liu, Z. C.; Xu, C. M.; Gao, J. S.; Zhuang, J.; Wang, X. *Chem.—Eur. J.* **2012**, *18*, 2639−2645.
(44) Amorim, C.; Keane, M. A. *J. Colloid Interface Sci.* **2008**, *322*, 196−208.
(45) Zheng, Z.; Gao, S.; Li, H.; Cao, R. *Chem. Commun.* **2010**, *46*, 6518−6520.
(46) Li, Y. N.; Jang, B. W.L. *Appl. Catal., A* **2011**, *392*, 173−179.
(47) Duca, D.; Arena, F.; Parmaliana, A.; Deganello, G. *Appl. Catal., A* **1998**, *172*, 207−216.
(48) Borodzínski, A. *Catal. Lett.* **2001**, *71*, 169−175.
(49) Ruta, M.; Semagina, N.; Kiwi-Minsker, L. *J. Phys. Chem. C* **2008**, *112*, 13635−13641.
(50) Xu, J.; Ouyang, L.; Mao, W.; Yang, X. J.; Xu, X. C.; Su, J. J.; Zhuang, T. Z.; Li, H.; Han, Y. F. *ACS Catal.* **2012**, *2*, 261−269.
(51) Shringarpure, P. A.; Patel, A. *Chem.—Eng. J.* **2011**, *173*, 612−619.
(52) Molero, H.; Bartlett, B. F.; Tysoe, W. T. *J. Catal.* **1999**, *181*, 49−56.
(53) Duca, D.; Frusteri, F.; Parmaliana, A.; Deganello, G. *Appl. Catal., A* **1996**, *146*, 269−284.
(54) Zaera, F. *Acc. Chem. Res.* **2009**, *42*, 1152−1160.
(55) Kim, W. J.; Kang, J. H.; Ahn, I. Y.; Moon, S. H. *J. Catal.* **2004**, *226*, 226−229.
(56) Zaera, F. *J. Mol. Catal. A* **2005**, *228*, 21−26.
(57) Delbecq, F.; Zaera, F. *J. Am. Chem. Soc.* **2008**, *130*, 14924−14925.
(58) Lee, I.; Zaera, F. *J. Phys. Chem. C* **2007**, *111*, 10062−10072.
(59) Hub, S.; Hilaire, L.; Touroude, R. *Appl. Catal.* **1988**, *36*, 307−322.
(60) Crespo-Quesada, M.; Yarulin, A.; Jin, M.; Xia, Y.; Kiwi-Minsker, L. *J. Am. Chem. Soc.* **2011**, *133*, 12787−12794.
(61) Kim, W. J.; Kang, J. H.; Ahn, I. Y.; Moon, S. H. *J. Catal.* **2004**, *226*, 226−229.
(62) Chinayon, S.; Mekasuwandumrong, O.; Praserthdam, P.; Panpranot, J. *Catal. Comm.* **2008**, *9*, 2297−2302.
(63) McKenna, F.; Anderson, J. *J. Catal.* **2011**, *281*, 231−240.
(64) McKenna, F. M.; Mantarosie, L.; Wells, R. P. K.; Hardacre, C.; Anderson, J. A. *Catal. Sci. Technol.* **2012**, *2*, 632−638.